Journal of Zhejiang University-SCIENCE A (Applied Physics & Engineering)
ISSN 1673-565X (Print); ISSN 1862-1775 (Online)
www.zju.edu.cn/jzus; www.springerlink.com
E-mail: jzus@zju.edu.cn

A semi-implicit three-step method based on SUPG finite element formulation for flow in lid driven cavities with different geometries*

Cheng HUANG, Dai ZHOU‡, Yan BAO

(*School of Naval Architecture, Ocean and Civil Engineering, Shanghai Jiao Tong University, Shanghai 200240, China*)

E-mail: ryanhuang@sjtu.edu.cn; zhoudai@sjtu.edu.cn; ybao@sjtu.edu.cn

Received Mar. 13, 2010; Revision accepted Nov. 5, 2010; Crosschecked Dec. 13, 2010

Abstract: A numerical algorithm using a bilinear or linear finite element and semi-implicit three-step method is presented for the analysis of incompressible viscous fluid problems. The streamline upwind/Petrov-Galerkin (SUPG) stabilization scheme is used for the formulation of the Navier-Stokes equations. For the spatial discretization, the convection term is treated explicitly, while the viscous term is treated implicitly, and for the temporal discretization, a three-step method is employed. The present method is applied to simulate the lid driven cavity problems with different geometries at low and high Reynolds numbers. The results compared with other numerical experiments are found to be feasible and satisfactory.

Key words: Semi-implicit three-step method, Streamline upwind/Petrov-Galerkin (SUPG) finite element method (FEM), Unsteady incompressible flows, Lid driven cavity problem

doi:10.1631/jzus.A1000098 **Document code:** A **CLC number:** TU3

1 Introduction

The finite element method (FEM) has been widely used for the solution of various fluid dynamics problems in recent decades, and appears to be a powerful tool especially for the solution of problems with complex geometry or boundary conditions. However, it is well known that the conventional Galerkin FEM often fails to obtain stable numerical solutions for fluid flows at high Reynolds numbers. To overcome this drawback, stabilized finite element formulations for the computation of steady or unsteady flows have been developed, including streamline upwind/Petrov-Galerkin (SUPG) formulations (Brooks and Hughes, 1982; Hughes and Tezduyar, 1984; Tezduyar and Ganjoo, 1986), Galerkin least square techniques (Hughes *et al.*, 1989; Franca and Frey, 1992), characteristic Galerkin methods (Zienkiewicz and Codina, 1995; Zienkiewicz *et al.*, 1995; Bao *et al*., 2010a; 2010b), finite calculus methods (Oñate, 1998; Oñate *et al*., 2007) and others (Brezzi *et al*., 1992; Hughes, 1995). Among these, the SUPG stabilization technique, introduced by Hughes *et al.* (1986) and then further developed by Tezduyar (2007a; 2007b), is believed to be an efficient stabilized scheme for the solution of compressible and incompressible fluid flow problems.

Another efficient FEM for the numerical simulation of unsteady incompressible fluid flows is the Taylor-Galerkin method developed by Donea *et al.* (1984) and Selmin *et al.* (1985). The basis of the Taylor-Galerkin method is the temporal discretization of unknowns in a Taylor expansion and a successive spatial discretization of the finite elements according to the conventional Galerkin FEM. In comparison with the conventional Galerkin FEM, the Taylor-Galerkin method has the desired properties of extended stability and improved phase accuracy.

‡ Corresponding author

* Project supported by the National Natural Science Foundation of China (No. 51078230), the Research Fund for the Doctoral Program of Higher Education of China (No. 200802480056), and the Key Project of Fund of Science and Technology Development of Shanghai (No. 10JC1407900), China

However, this approach, though correct and easy to implement for the solution of unsteady fluid flows, would lead to a rather time-consuming formulation, since the second-order scheme of the Taylor-Galerkin method can be used only when the Courant number C_γ is less than $1/\sqrt{3}$.

Based on the Taylor-Galerkin method, a three-step FEM has been developed by Jiang and Kawahara (1993), and has proved to be cost-effective for incompressible flows, since it allows less frequent updates of the pressure field with good accuracy. In their studies, a stability analysis of the 1D purely convection equation is described. The results show that the three-step method is stable when the Courant number C_γ satisfies $0 \le C_\gamma \le 1$, and has third-order accuracy and an extended stability domain in comparison with the Lax-Wendroff FEM (Jiang and Kawahara, 1993).

In this paper we are concerned with an unsteady incompressible Newtonian fluid flow governed by the Navier-Stokes equations. For the modeling of the fluid flow we use the SUPG finite element formulation with the same order interpolations based on bilinear or linear elements for both the velocity and pressure. Therefore, the spatial discretization of the momentum equation is performed using the SUPG stabilized Galerkin method. The Poisson type pressure equation is derived from the incompressible constraint, and discretized using the standard Galerkin method. To avoid the diffusive time step restriction, the diffusive terms are solved implicitly and convective terms explicitly. For the temporal integration of Navier-Stokes equations, we use the three-step method, in which the time step is divided into equal three substeps, hence, fully discretized finite element schemes of considered fluid flow problems are obtained.

For the verification of the proposed algorithm, numerical tests for lid driven cavity flow problems are presented: the lid driven flows are in a square, a triangular, and a skewed cavity at low and high Reynolds numbers. The present results are shown to be accurate compared with other numerical results.

2 Incompressible Navier-Stokes equations

We consider the following velocity-pressure formulation of the Navier-Stokes equations written in the Eulerian form for unsteady incompressible flows:

$$\frac{\partial u_i}{\partial t} + u_j u_{i,j} = \sigma_{ij,j} + f_i, \quad \text{in } \Omega \times [0,T], \tag{1}$$

$$u_{i,i} = 0, \quad \text{in } \Omega \times [0,T], \tag{2}$$

where Ω, $[0,T]$ are the spatial and temporal domains, u_i is the i-component velocity, f_i is the external force, t is the time. The subscript ',' denotes spatial derivative; i.e., $u_{i,j}$ denotes the derivative of u_i to j direction. σ_{ij} is the stress tensor given by

$$\sigma_{ij} = -p\delta_{ij}/\rho + \nu(u_{i,j} + u_{j,i}), \tag{3}$$

where p and ν are the pressure and kinematic viscosity, ρ is the fluid density, and δ_{ij} represents the identity tensor. The boundary conditions are

$$u_i = g_i, \quad \text{on } \Gamma_g, \tag{4}$$

$$\sigma_{ij} n_j = h_i, \quad \text{on } \Gamma_h, \tag{5}$$

where Γ_g and Γ_h are two disjoint subsets of the boundary Γ, g_i and h_i are the prescribed values on the boundary, and n_j is the j-component of the unit vector normal to the boundary.

3 Semi-implicit three-step method

The governing equations are integrated in time using a semi-implicit three-step method. In this method, the convection term is treated explicitly, whereas the viscous term is treated implicitly. The momentum equations at each of the substeps are then discretized as follows:

$$\frac{u_i^{n+1/3} - u_i^n}{\Delta t/3} = -u_j^n u_{i,j}^n - p_{,i}^n/\rho + \nu(\beta u_{i,jj}^n + (1-\beta)u_{i,jj}^{n+1/3}) + f_i^n, \tag{6a}$$

$$\frac{u_i^{n+2/3} - u_i^{n+1/3}}{\Delta t/3} = -u_j^{n+1/3} u_{i,j}^{n+1/3} - p_{,i}^n/\rho + \nu(\beta u_{i,jj}^{n+1/3} + (1-\beta)u_{i,jj}^{n+2/3}) + f_i^{n+1/3}, \tag{6b}$$

$$\frac{u_i^{n+1} - u_i^{n+2/3}}{\Delta t/3} = -u_j^{n+2/3} u_{i,j}^{n+2/3} - p_{,i}^{n+1}/\rho + \nu(\beta u_{i,jj}^{n+2/3} + (1-\beta)u_{i,jj}^{n+1}) + f_i^{n+2/3}, \tag{6c}$$

where $u_{i,jj}$ is the second derivative of u_i to j direction, and $p_{,i}$ is the derivative of p to i direction. Δt is the time increment, and the superscript 'n' denotes the time level. The implicitness in the numerical scheme is introduced with β=0.5, and thus, the second-order accurate implicit trapezoid method for the viscous term is obtained (Kjellgren, 1997). As a result, the time increment of the semi-implicit method will not be restricted by the viscous limit.

4 Finite element formulation of the governing equations

4.1 SUPG finite element formulation of the Navier-Stokes equations

By multiplying the velocity test function and integrating over the computational domain Ω, and with the added SUPG stabilization term, the weak form of the momentum Eq. (1) is achieved as follows (Brooks and Hughes, 1982; Hughes and Tezduyar, 1984; Tezduyar and Ganjoo, 1986):

$$\int_{\Omega}\left[\delta u_i\left(\frac{\partial u_i}{\partial t}+u_j u_{i,j}-f_i\right)+\sigma_{ij}\delta u_{i,j}\right]\mathrm{d}\Omega-\int_{\Gamma^h}h_i\delta u_i\mathrm{d}\Gamma$$
$$+\sum_{e=1}^{n_{\mathrm{el}}}\int_{\Omega^e}\tau_{\mathrm{SUPG}}u_j\delta u_{i,j}\left(\frac{\partial u_i}{\partial t}+u_j u_{i,j}-\sigma_{ij,j}-f_i\right)\mathrm{d}\Omega=0, \tag{7}$$

where n_{el} is the number of elements, Ω^e is the domain of single element, δu_i is the velocity test function, and the stabilization parameter τ_{SUPG} is defined as (Dettmer and Perić, 2006a; 2006b; 2006c)

$$\tau_{\mathrm{SUPG}}=\frac{h^e}{2\left\|u^e\right\|\rho}z,$$
$$z=\frac{\beta_1}{\sqrt{1+\left(\dfrac{\beta_1}{\beta_2 Re^e}\right)^2}},\ Re^e=\frac{\left\|u^e\right\|h^e}{2\nu}, \tag{8}$$

where h^e, u^e, and Re^e represent, respectively, the characteristic element size, the convective velocity in the element centroid, and the element Reynolds number. z is the process parameter. The parameters β_1 and β_2 define the limits of z as $Re^e\to\infty$ and the derivative $\dfrac{\mathrm{d}z}{\mathrm{d}Re^e}$ at Re^e=0, respectively. The numerical examples in this study have all been obtained with β_1=1 and β_2=1/3. In this work, the characteristic element size h^e is defined as the diameter of the circle, the area of which corresponds to the element e.

The spatial discretization process using the FEM follows the procedures of Belytschko *et al*. (2000). The same order interpolations based on bilinear or linear elements are used for both the velocity and pressure. Thus, u_i and p, along with the test functions δu_i and δp, are expressed as follows:

$$u_i=\sum_I \Phi_I u_{iI}, \tag{9a}$$
$$p=\sum_I \Phi_I p_I, \tag{9b}$$
$$\delta u_i=\Phi_I, \tag{9c}$$
$$\delta p=\Phi_I, \tag{9d}$$

where Φ_I is the nodal shape function at node I, and u_{iI} and p_I are the values of u_i and p at node I in a single element, respectively.

Substituting the interpolations into Eq. (7), and applying the semi-implicit three-step method, we derive the resulting finite element formulations of momentum equations:

$$M_{IJ}^n\frac{u_{iJ}^{n+1/3}-u_{iJ}^n}{\Delta t/3}=-N_{IJ}^n u_{iJ}^n+G_{iIJ}^n p_J^n/\rho$$
$$-\frac{\nu}{2}(S_{IJ}^n u_{iJ}^n+S_{IJ}^{n+1/3}u_{iJ}^{n+1/3})$$
$$+D_{iI}^n-E_{iI}^n/\rho+F_{iI}^n, \tag{10}$$

$$M_{IJ}^{n+1/3}\frac{u_{iJ}^{n+2/3}-u_{iJ}^{n+1/3}}{\Delta t/3}=-N_{IJ}^{n+1/3}u_{iJ}^{n+1/3}+G_{iIJ}^{n+1/3}p_J^n/\rho$$
$$-\frac{\nu}{2}(S_{IJ}^{n+1/3}u_{iJ}^{n+1/3}+S_{IJ}^{n+2/3}u_{iJ}^{n+2/3})+D_{iI}^{n+1/3}$$
$$-E_{iI}^n/\rho+F_{iI}^{n+1/3}, \tag{11}$$

$$M_{IJ}^{n+2/3}\frac{u_{iJ}^{n+1}-u_{iJ}^{n+2/3}}{\Delta t/3}=-N_{IJ}^{n+2/3}u_{iJ}^{n+2/3}+G_{iIJ}^{n+2/3}p_J^{n+1}/\rho$$
$$-\frac{\nu}{2}(S_{IJ}^{n+2/3}u_{iJ}^{n+2/3}+S_{IJ}^{n+1}u_{iJ}^{n+1})$$
$$-\frac{\nu}{2}(S_{IJ}^{n+2/3}u_{iJ}^{n+2/3}+S_{IJ}^{n+1}u_{iJ}^{n+1})+D_{iI}^{n+2/3}$$
$$-E_{iI}^{n+1}/\rho+F_{iI}^{n+2/3}, \tag{12}$$

where $M_{IJ}^{n+\theta}$, $N_{IJ}^{n+\theta}$, $G_{iIJ}^{n+\theta}$, $F_{iI}^{n+\theta}$, $D_{iI}^{n+\theta}$, $S_{IJ}^{n+\theta}$, and $E_{iI}^{n+\theta}$ are defined as

$$M_{IJ}^{n+\theta}=\int_{\Omega^e}\Phi_I\Phi_J\mathrm{d}\Omega+\int_{\Omega^e}\tau_{\mathrm{SUPG}}u_{iK}^{n+\theta}\Phi_K\Phi_{I,i}\Phi_J\mathrm{d}\Omega, \tag{13a}$$

$$N_{IJ}^{n+\theta}=\int_{\Omega^e}\Phi_I u_{iK}^{n+\theta}\Phi_K\Phi_{J,i}\mathrm{d}\Omega+\int_{\Omega^e}\tau_{\mathrm{SUPG}}u_{iK}^{n+\theta}\Phi_K\Phi_{I,i}u_{jL}^{n+\theta}\Phi_L\Phi_{J,j}\mathrm{d}\Omega, \tag{13b}$$

$$G_{iIJ}^{n+\theta}=\int_{\Omega^e}\Phi_{I,i}\Phi_J\mathrm{d}\Omega-\int_{\Omega^e}\tau_{\mathrm{SUPG}}u_{jK}^{n+\theta}\Phi_K\Phi_{I,j}\Phi_{J,i}\mathrm{d}\Omega, \tag{13c}$$

$$F_{iI}^{n+\theta}=\int_{\Gamma^e}\nu\Phi_I\Phi_{J,j}u_{iJ}^{n+\theta}n_j\mathrm{d}\Gamma, \tag{13d}$$

$$D_{iI}^{n+\theta}=\int_{\Omega^e}\Phi_I f_i\mathrm{d}\Omega+\int_{\Omega^e}\tau_{\mathrm{SUPG}}u_{jK}^{n+\theta}\Phi_K\Phi_{I,j}f_i\mathrm{d}\Omega, \tag{13e}$$

$$S_{IJ}^{n+\theta}=\int_{\Omega^e}\Phi_{I,j}\Phi_{J,j}\mathrm{d}\Omega, \tag{13f}$$

$$E_{iI}^{n+\theta}=\int_{\Gamma^e}\Phi_I p^{n+\theta}n_i\mathrm{d}\Gamma, \tag{13g}$$

where subscripts '*I*', '*J*', '*K*' and '*L*' are denoted as node indexes, and '*i*', '*j*' are space indexes; and the parameter θ is set to different values (0, 1/3, and 2/3 for Eqs. (13a)–(13e); 0, 1/3, 2/3, 1 for Eq. (13f); 0, and 1 for Eq. (13g)).

4.2 Finite element formulation of the pressure equation

The weak form of the pressure equation is obtained by multiplying the continuity equation by the pressure test function δp and applying the divergence theorem, and can be expressed as follows:

$$\int_\Omega\delta p_{,i}u_i\mathrm{d}\Omega-\int_{\Gamma^g}\delta pg_in_i\mathrm{d}\Gamma=0. \tag{14}$$

To obtain the Poisson type pressure equation from the continuity constraint, we discretize Eq. (1) at the time level $t=t^{n+1/2}$, and then, the following equation can be obtained:

$$\frac{u_i^{n+1}}{\Delta t}=\frac{u_i^n}{\Delta t}-u_j^{n+1/2}u_{i,j}^{n+1/2}-p_{,i}^{n+1}/\rho+\nu u_{i,jj}^{n+1/2}+f_i^{n+1/2}. \tag{15}$$

Substituting Eq. (15) into Eq. (14), the Poisson type pressure equation can be expressed as

$$\begin{aligned}\int_\Omega\delta p_{,i}p_{,i}^{n+1}/\rho\mathrm{d}\Omega=&\frac{1}{\Delta t}\int_\Omega\delta p_{,i}u_i^n\mathrm{d}\Omega\\&-\int_\Omega\delta p_{,i}u_j^{n+1/2}u_{i,j}^{n+1/2}\mathrm{d}\Omega+\int_\Omega\delta p_{,i}f_i^{n+1/2}\mathrm{d}\Omega\\&+\int_\Omega\delta p_{,i}\nu u_{i,jj}^{n+1/2}\mathrm{d}\Omega-\frac{1}{\Delta t}\int_{\Gamma^g}\delta pg_i^{n+1}n_i\mathrm{d}\Gamma.\end{aligned} \tag{16}$$

Since the interpolation based on linear or bilinear elements is used for velocity, the viscous term in Eq. (16) has vanished, and using the divergence theorem, Eq. (16) can be rewritten as

$$\begin{aligned}\int_\Omega\delta p_{,i}p_{,i}^{n+1}/\rho\mathrm{d}\Omega=&-\frac{1}{\Delta t}\int_\Omega\delta pu_{i,i}^n\mathrm{d}\Omega\\&-\int_\Omega\delta p_{,i}u_j^{n+1/2}u_{i,j}^{n+1/2}\mathrm{d}\Omega+\int_\Omega\delta p_{,i}f_i^{n+1/2}\mathrm{d}\Omega\\&-\frac{1}{\Delta t}\int_{\Gamma^g}\delta p(g_i^{n+1}-g_i^n)n_i\mathrm{d}\Gamma,\end{aligned} \tag{17}$$

where

$$u_i^{n+1/2}=\frac{1}{2}(u_i^{n+1/3}+u_i^{n+2/3}), \tag{18}$$

where the velocities $u_i^{n+1/3}$ and $u_i^{n+2/3}$ are calculated by Eqs. (10) and (11), respectively.

Substituting the expressions of trial and test functions Eqs. (9a)–(9d) into Eq. (17), the final finite element formulation of the Poisson type equation is

$$H_{IJ}p_J^{n+1}=-Q_{iIJ}u_{iJ}^n-R_{iIJ}u_{iJ}^{n+1/2}-P_I+W_I, \tag{19}$$

where

$$H_{IJ}=\frac{1}{\rho}\int_{\Omega^e}\Phi_{I,i}\Phi_{J,i}\mathrm{d}\Omega, \tag{20a}$$

$$Q_{iIJ}=\frac{1}{\Delta t}\int_{\Omega^e}\Phi_I\Phi_{J,i}\mathrm{d}\Omega, \tag{20b}$$

$$R_{iIJ}=\int_{\Omega^e}\Phi_{I,j}\Phi_J\Phi_{K,i}u_{jK}^{n+1/2}\mathrm{d}\Omega, \tag{20c}$$

$$P_I=\frac{1}{\Delta t}\int_{\Gamma^e}\Phi_I(g_i^{n+1}-g_i^n)n_i\mathrm{d}\Gamma, \tag{20d}$$

$$W_I=\int_{\Omega^e}\Phi_{I,i}f_i^{n+1/2}\mathrm{d}\Gamma. \tag{20e}$$

5 Numerical examples

In this section, lid driven flow problems of low and high Reynolds numbers in a square, a triangular,

and a skewed cavity are considered to verify the present numerical method. A standard iteration process, biconjugate gradient solver (BICGS) was employed to solve the linear system, which results from the finite element discretization described above. For the solution of high Reynolds numbers, the converged solution of lower Reynolds number was used as an initial guess, and found to be in good agreement with previous numerical solutions (Kohno and Bathe, 2006). All the numerical results are nondimensionalized described.

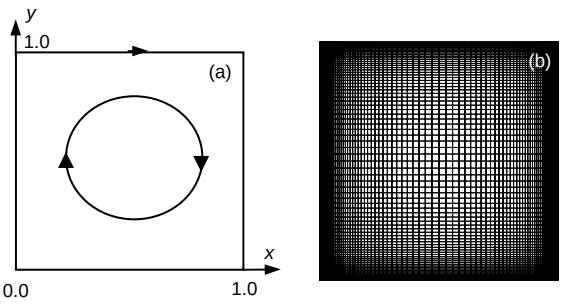

Fig. 1 Square cavity flow problem definition (a) and nonuniform grid system (b)

5.1 Lid driven flow in a square cavity

Fig. 1 shows the schematics of a square cavity flow with a coordinate system and a nonuniform mesh with 80×80 quadrilateral bilinear elements for the problem. A unit horizontal velocity is prescribed on the top lid, while the no-slip boundary condition is imposed on all other sides and on the corners of the top lid. In addition, zero pressure is prescribed on the left corner of the bottom side. Calculations of the flows of Reynolds numbers 1000, 5000, and 7500 were performed. In all cases, the time step Δt=0.01 was used, and the corresponding maximum Courant number was 2.78, which is defined as

$$C_\gamma = \frac{\Delta t u^e}{h^e}. \tag{21}$$

Figs. 2 and 3 show the horizontal and vertical velocity profiles, respectively, along the vertical centerline (0.5, y), and the horizontal centerline (x, 0.5) for Re=1000, 5000, and 7500. Figs. 4–7 show the velocity distributions, pressure contours, streamline patterns, and vorticity contours of the steady-state results for Re=1000, 5000, and 7500, respectively. The present numerical results are in good agreement with the solutions of Ghia *et al*. (1982).

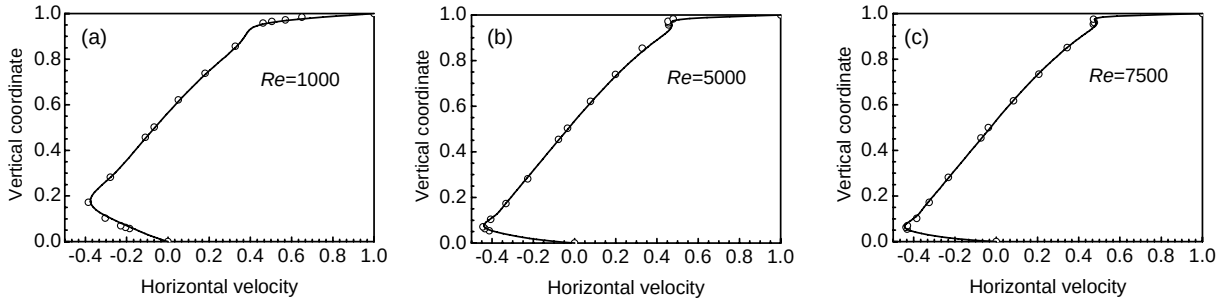

Fig. 2 Horizontal velocity profiles along the centerline for *Re*=1000 (a), *Re*=5000 (b), and *Re*=7500 (c)
Solid line: current results; circles: results given in (Ghia *et al.*, 1982)

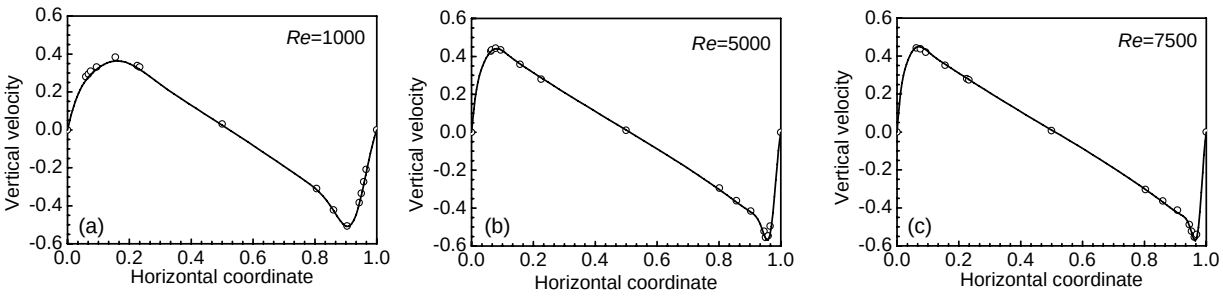

Fig. 3 Vertical velocity profiles along the centerline for *Re*=1000 (a), *Re*=5000 (b), and *Re*=7500 (c)
Solid line: current results; circles: results given in (Ghia *et al.*, 1982)

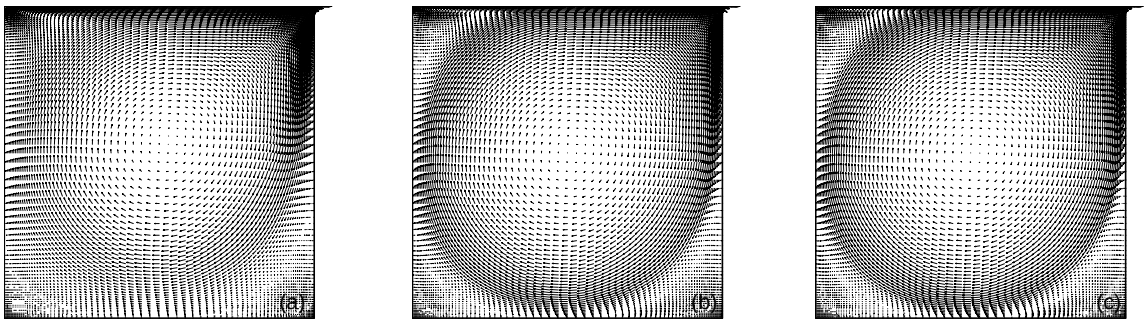

Fig. 4 Velocity distributions for *Re*=1000 (a), *Re*=5000 (b), and *Re*=7500 (c)

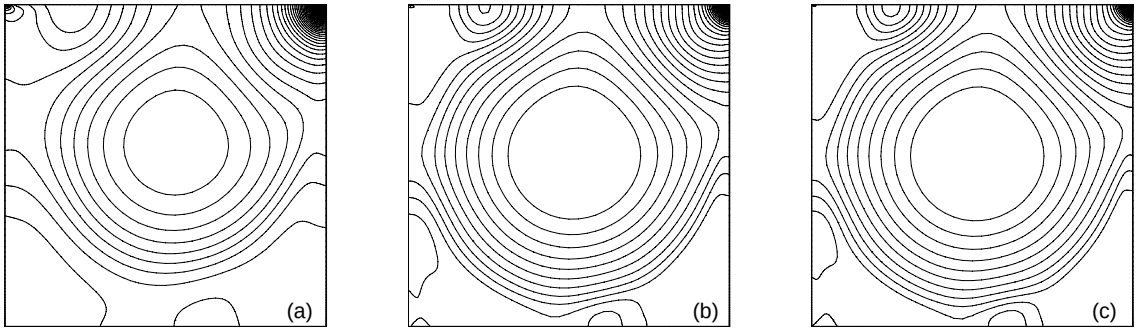

Fig. 5 Pressure contours for *Re*=1000 (a), *Re*=5000 (b), and *Re*=7500 (c)

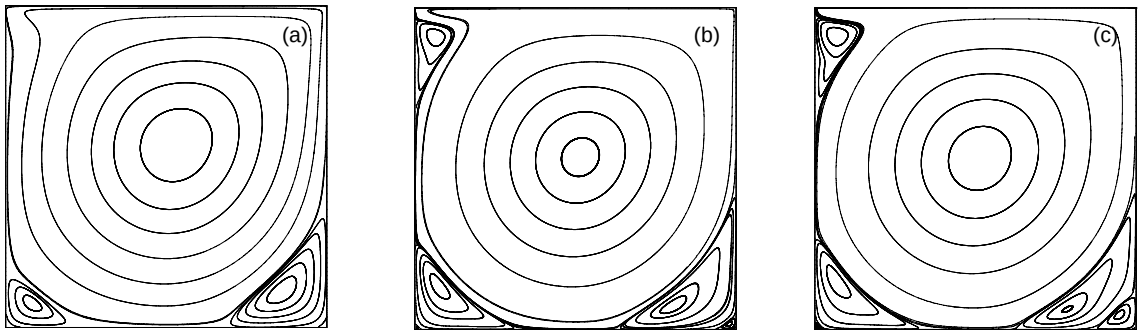

Fig. 6 Streamline patterns for *Re*=1000 (a), *Re*=5000 (b), and *Re*=7500 (c)

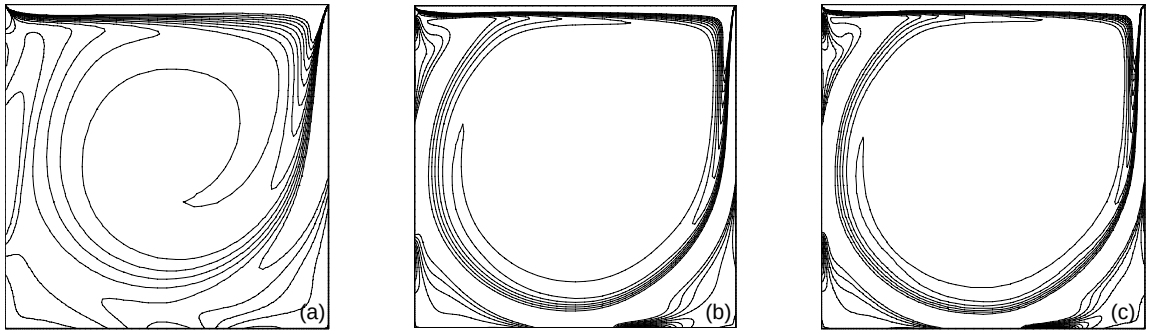

Fig. 7 Vorticity contours for *Re*=1000 (a), *Re*=5000 (b), and *Re*=7500 (c)

5.2 Lid driven flow in a triangular cavity

In this problem we consider the lid driven flows in an isosceles triangular cavity with the same geometry and boundary conditions as in Ribbens and Watson (1994), Jyotsna and Vanka (1995), and Kohno and Bathe (2006). Figs. 8a–8c show the geometry of the triangular cavity with the coordinate system and the nomenclature for the vortices. To obtain a more accurate solution, we used an irregular grid system with 12 046 triangular linear elements (Fig. 8c). The boundary conditions imposed were as follows: a unit horizontal velocity is prescribed on the top lid, while no-slip boundary condition is imposed on the left and right sides of the triangular cavity and on the corners of the top lid. As for the triangular cavity problem, zero pressure is prescribed at the bottom corner of the cavity. The steady state solutions were obtained for the cases Re=100, 500, and 1000 using the time increment Δt=0.02 with the corresponding maximum Courant number C_γ=2.17.

Figs. 9 and 10 show the velocity profiles along the vertical centerline (x=0) and horizontal line (y=−1), respectively, for the cases Re=100, 500, and 1000. Figs. 11–14 show the velocity distributions,

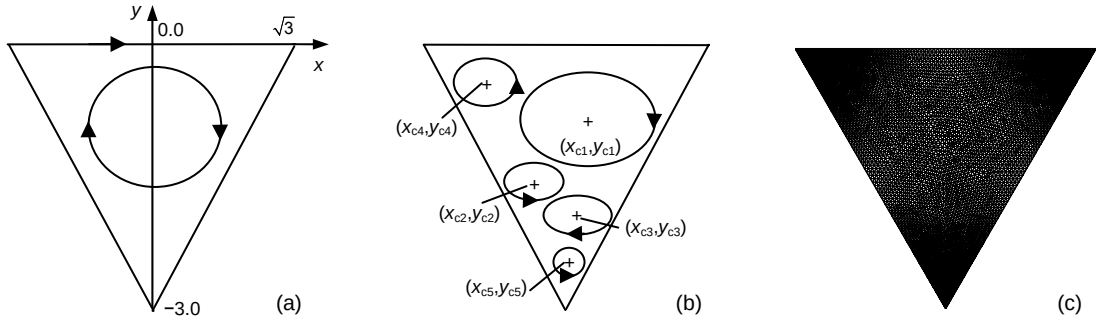

Fig. 8 Triangular cavity flow problem definition (a), nomenclature (Kohno and Bathe, 2006) (b), and unstructured grid system with 12 046 elements (c)

'+' denotes the vortex center positions, and (x_{c1},y_{c1}), (x_{c2},y_{c2}), (x_{c3},y_{c3}), (x_{c4},y_{c4}), and (x_{c5},y_{c5}) are the coordinates of vortex center positions

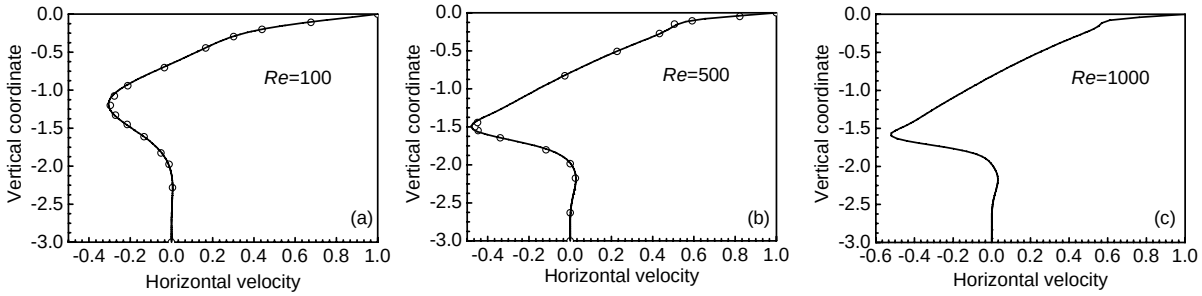

Fig. 9 Horizontal velocity profiles along the centerline for *Re*=100 (a), *Re*=500 (b), and *Re*=1000 (c)

Solid line: current results; circles: results in Kohno and Bathe (2006)

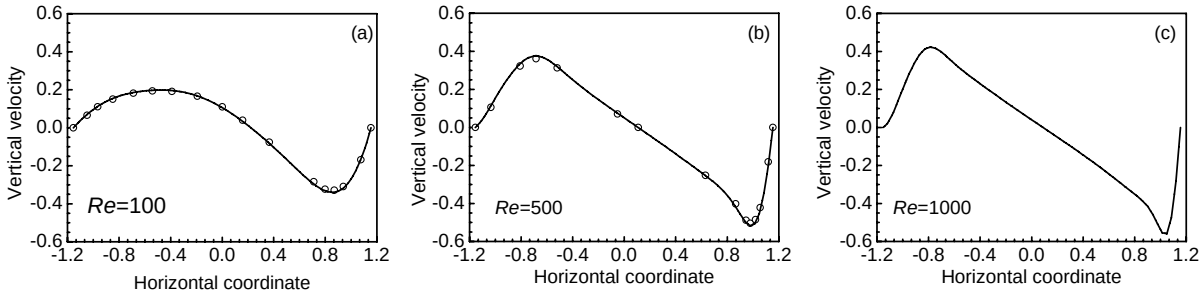

Fig. 10 Vertical velocity profiles along the line y=−1 for *Re*=100 (a), *Re*=500 (b), and *Re*=1000 (c)

Solid line: current results; circles: results in Kohno and Bathe (2006)

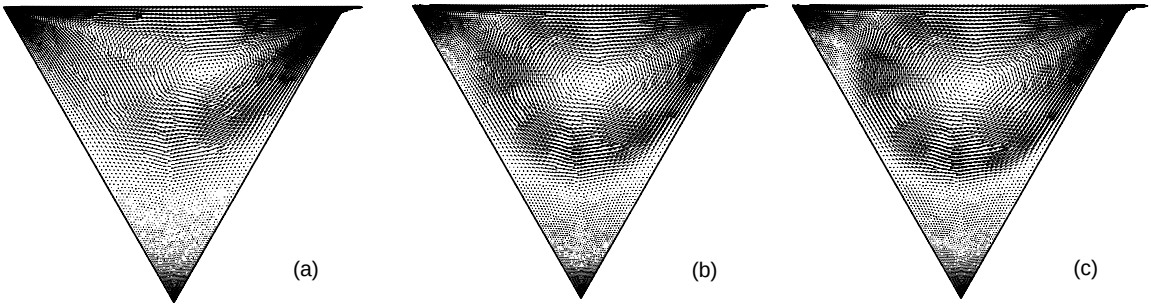

Fig. 11 Velocity distributions for *Re*=100 (a), *Re*=500 (b), and *Re*=1000 (c)

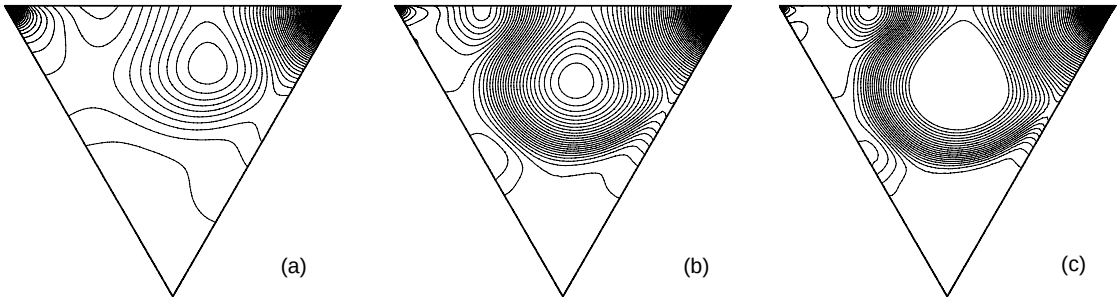

Fig. 12 Pressure contours for *Re*=100 (a), *Re*=500 (b), and *Re*=1000 (c)

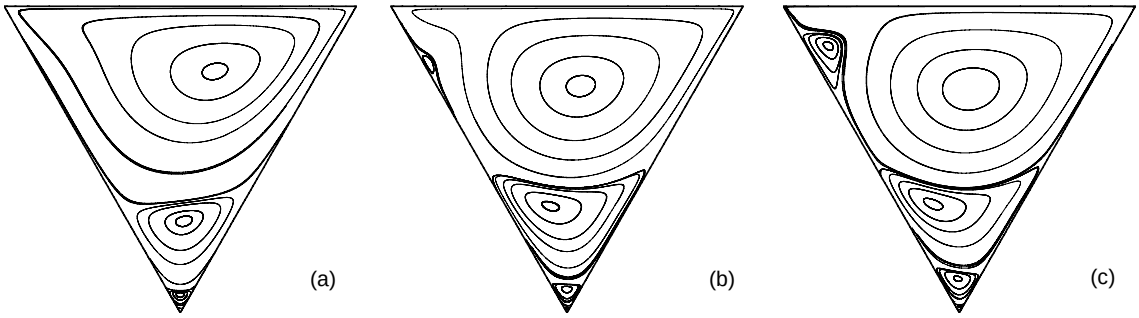

Fig. 13 Streamline patterns for *Re*=100 (a), *Re*=500 (b), and *Re*=1000 (c)

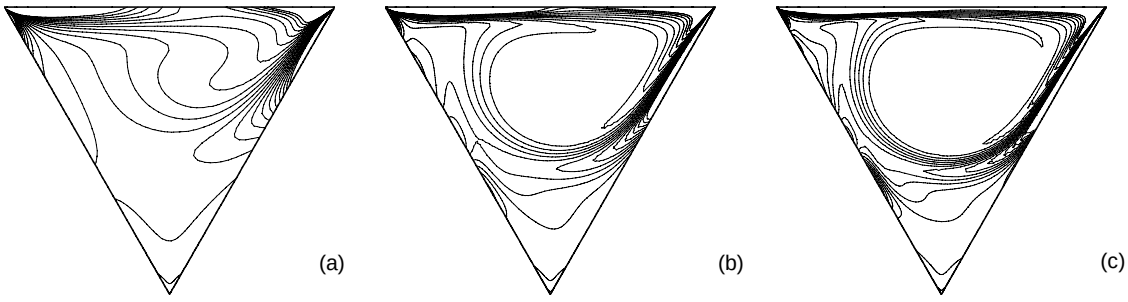

Fig. 14 Vorticity contours for *Re*=100 (a), *Re*=500 (b), and *Re*=1000 (c)

pressure contours, streamline patterns, and vorticity contours, respectively, for all the cases. The center locations of the vortices according to the nomenclature in Fig. 8b are compared with that of Kohno and Bathe (2006) in Table 1. The present results are in good agreement with those of Kohno and Bathe (2006).

5.3 Lid driven flow in a skewed cavity

In the third fluid flow example, we consider the numerical solution of driven flows in a skewed cavity with a skew angle of 45°, as first proposed by Demirdžić *et al*. (1992), at two different Reynolds number values, *Re*=100 and 1000. In this study, we consider flow conditions of *Re*=100, 1000, 5000, and 7500, and grids with uniform node distributions of 151×151 and with 45 000 triangular elements for all the Reynolds numbers considered. Fig. 15a illustrates a schematic view of the skewed cavity problem with the coordinate system, and Fig. 15b shows the element patterns of the regular mesh used for the solution of the problem. Prescribed boundary conditions were as follows: zero velocity at the walls and bottom, a unit horizontal velocity at the cavity top, and zero pressure at the left corner of the cavity top. In this analysis, time step Δt=0.01 was used for all the cases of different Reynolds numbers, and its corresponding maximum Courant number C_γ was 1.51.

Figs. 16 and 17 present the horizontal and vertical velocity component profiles along the centerlines CL_2 and CL_1 (Fig. 15a), respectively, obtained by the present method at all the Reynolds numbers, in comparison with the results given by Demirdžić *et al*. (1992) for *Re*=100 and 1000. Predicted streamlines and vorticity contours for flow cases are shown in Figs. 18 and 19, and the positions of the primary vortex and secondary vortex are presented in Table 2 compared Demirdžić *et al*. (1992). With an increase in Reynolds number, the secondary vortex becomes larger and larger, while the primary vortex size reduces, and when the *Re* reaches 5000, a vortex appears at the right side of the cavity, and its size increases with the increase of *Re*.

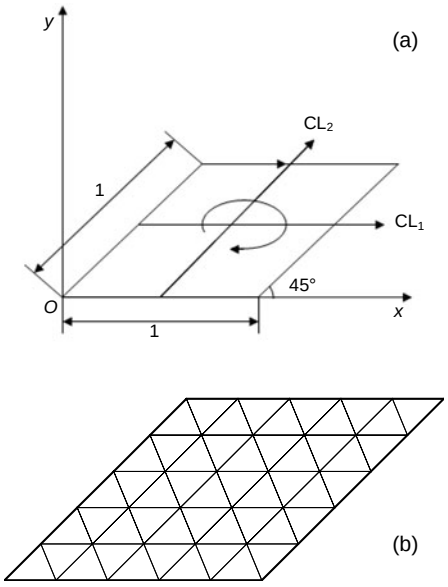

Fig. 15 Skewed cavity flow problem definition (a) and element patterns of regular mesh (b)

Table 1 Comparison of vortex center positions in the triangular cavity problem

Group	(x_{c1},y_{c1})	(x_{c2},y_{c2})	(x_{c3},y_{c3})	(x_{c4},y_{c4})	(x_{c5},y_{c5})
Re=100					
Present method	(0.3410,−0.6381)	(0.0367,−2.1057)	(0.0002,−2.8230)	−	−
Kohno and Bathe (2006)	(0.3467,−0.6416)	(0.0382,−2.1146)	(0.0002,−2.8254)	−	−
Re=500					
Present method	(0.1348,−0.7841)	(−0.1649,−1.9561)	(−0.0020,−2.7730)	(−1.3524,−0.5532)	(0.0000,−2.9591)
Kohno and Bathe (2006)	(0.1391,−0.7864)	(−0.1580,−1.9631)	(−0.0022,−2.7716)	(−1.3484,−0.5538)	−
Re=1000					
Present method	(0.1106,−0.8077)	(−0.2622,−1.9357)	(−0.0154,−2.6657)	(−1.2881,−0.3856)	(0.0002,−2.9348)
Kohno and Bathe (2006)	(0.1113,−0.8143)	(−0.2561,−1.9458)	(−0.0163,−2.6628)	(−1.2844,−0.3864)	−

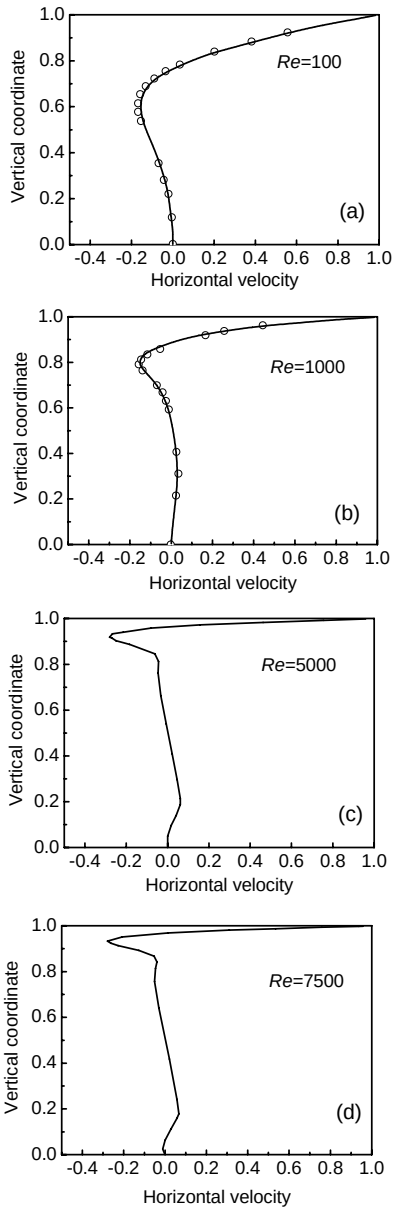

Fig. 16 Horizontal velocity profiles along the centerline CL_2 for *Re*=100 (a), *Re*=1000 (b), *Re*=5000 (c), and *Re*=7500 (d)

Solid line: current results; circles: results in Demirdžić *et al*. (1992)

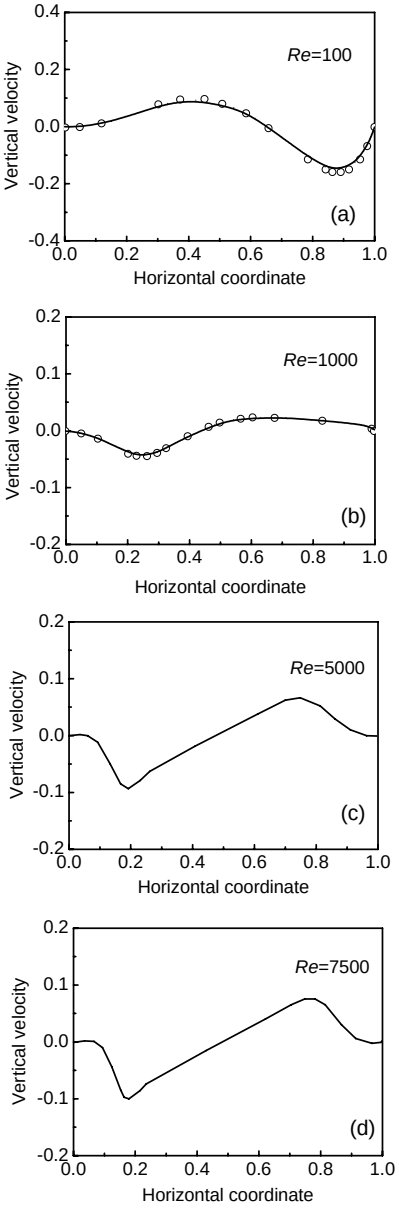

Fig. 17 Vertical velocity profiles along the centerline CL_1 for *Re*=100(a), *Re*=1000 (b), *Re*=5000 (c), and *Re*=7500 (d)

Solid line: current results; circles: results in Demirdžić *et al*. (1992)

Table 2 Comparison of primary and secondary vortex center positions in the skewed cavity problem

	Group	Primary vortex center position	Secondary vortex center position
Re=100	Present method	(1.1170,0.5459)	(0.3395,0.1425)
	Demirdžić *et al.* (1992)	(1.1100,0.5464)	(0.3387,0.1431)
Re=1000	Present method	(1.3244,0.5783)	(0.7823,0.3998)
	Demirdžić *et al.* (1992)	(1.3130,0.5740)	(0.7766,0.3985)
Re=5000	Present method	(1.5139,0.6407)	(0.8246,0.3619)
Re=7500	Present method	(1.5488,0.6524)	(0.8319,0.3607)

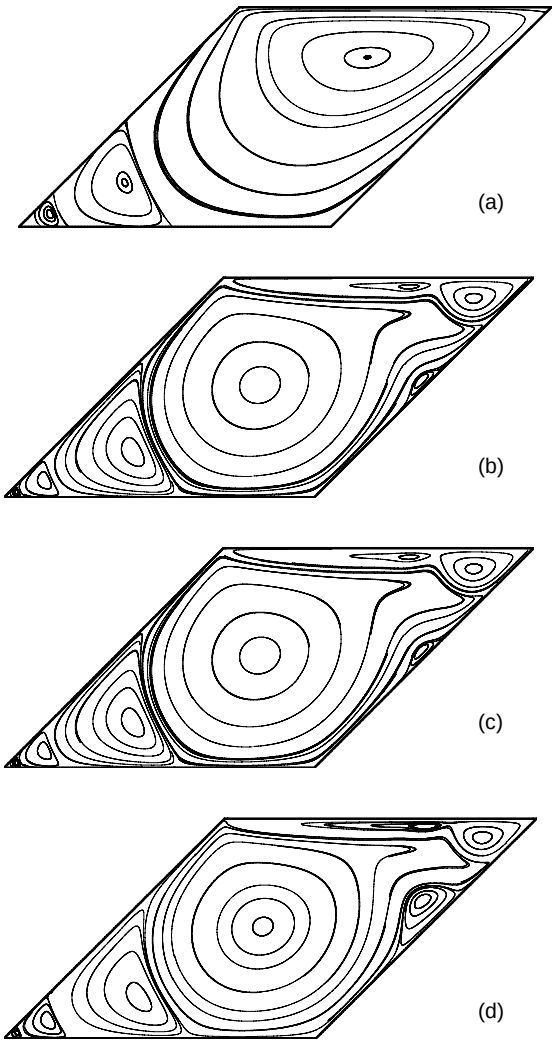

Fig. 18 Streamline patterns for *Re*=100 (a), *Re*=1000 (b), *Re*=5000 (c), and *Re*=7500 (d)

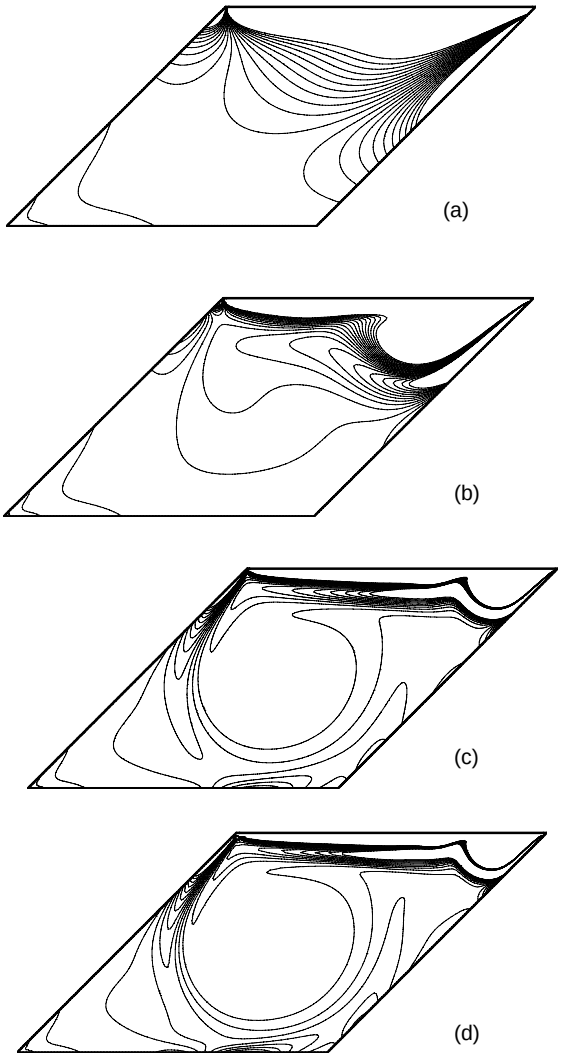

Fig. 19 Vorticity contours for *Re*=100 (a), *Re*=1000 (b), *Re*=5000 (c), and *Re*=7500 (d)

6 Conclusions

In this paper we presented a numerical algorithm which used a semi-implicit three-step method accommodating stabilized bilinear and linear equal-order interpolation velocity-pressure elements. The SUPG stabilization technique was employed for the formulation of Navier-Stokes equations. Since there are no restrictions on time step due to the diffusion term, the present scheme allows larger Courant numbers for the solution of unsteady incompressible viscous flow problems. Results from our numerical tests showed good agreement with those reported in previous studies (Ghia *et al*., 1982; Demirdžić *et al*., 1992; Kohno and Bathe, 2006) and suggest that the present method is competitive for the solution of incompressible viscous flows in terms of both accuracy and efficiency.

References

Bao, Y., Zhou, D., Zhao, Y.Z., 2010a. A two-step taylor-characteristic-based Galerkin method for incompressible flows and its application to flow over triangular cylinder with different incidence angles. *International Journal for Numerical Methods in Fluids*, **62**(11):1181-1208. [doi:10.1002/fld.2054]

Bao, Y., Zhou, D., Huang, C., 2010b. Numerical simulation of flow over three circular cylinders in equilateral arrangements at low Reynolds number by a second-order

characteristic-based split finite element method. *Computers & Fluids*, **39**(5):882-899. [doi:10.1016/j.compfluid.2010.01.002]

Belytschko, T.B., Liu, W.K., Moran, B., 2000. Nonlinear Finite Elements for Continua and Structures. Wiley, Chichester.

Brezzi, F., Bristeau, M.O., Franca, L.P., Mallet, M., Roge, G., 1992. A relationship between stabilized finite element methods and the Galerkin method with bubble functions. *Computer Methods in Applied Mechanics and Engineering*, **96**(1):117-129. [doi:10.1016/0045-7825(92)90102-P]

Brooks, A.N., Hughes, T.J.R., 1982. Streamline upwind/Petrov-Galerkin formulation for convection dominated flows with particular emphasis on the incompressible Navier-Stokes equations. *Computer Methods in Applied Mechanics and Engineering*, **32**(1-3):199-259. [doi:10.1016/0045-7825(82)90071-8]

Demirdžić, I., Lilek, Ž., Perić, M., 1992. Fluid flow and heat transfer test problems for non-orthogonal grids: benchmark solutions. *International Journal for Numerical Methods in Fluids*, **15**(3):329-354. [doi:10.1002/fld.1650150306]

Dettmer, W., Perić, D., 2006a. A computational framework for fluid-rigid body interaction: Finite element formulation and applications. *Computer Methods in Applied Mechanics and Engineering*, **195**(13-16):1633-1666. [doi:10.1016/j.cma.2005.05.033]

Dettmer, W., Perić, D., 2006b. A computational framework for free surface fluid flows accounting for surface tension. *Computer Methods in Applied Mechanics and Engineering*, **195**(23-24):3038-3071. [doi:10.1016/j.cma.2004.07.057]

Dettmer, W., Perić, D., 2006c. A computational framework for fluid-structure interaction: Finite element formulation and applications. *Computer Methods in Applied Mechanics and Engineering*, **195**(41-43):5754-5779. [doi:10.1016/j.cma.2005.10.019]

Donea, J., Giuliani, S., Laval, H., Quartapelle, L., 1984. Time-accurate solution of advection-diffusion problems by finite elements. *Computer Methods in Applied Mechanics and Engineering*, **45**(1-3):123-145. [doi:10.1016/0045-7825(84)90153-1]

Franca, L.P., Frey, S.L., 1992. Stabilized finite element methods: II. The incompressible Navier-Stokes equations. *Computer Methods in Applied Mechanics and Engineering*, **99**(2-3):209-233. [doi:10.1016/0045-7825(92)90041-H]

Ghia, U., Ghia, K.N., Shin, C.T., 1982. High-*Re* solutions for incompressible flow using the Navier-Stokes equations and a multigrid method. *Journal of Computational Physics*, **48**(3):387-411. [doi:10.1016/0021-9991(82)90058-4]

Hughes, T.J.R., 1995. Multiscale phenomena: Greens functions subgrid scale models, bubbles and the origins of stabilized methods. *Computer Methods in Applied Mechanics and Engineering*, **127**(1-4):387-401. [doi:10.1016/0045-7825(95)00844-9]

Hughes, T.J.R., Tezduyar, T.E., 1984. Finite element methods for first-order hyperbolic systems with particular emphasis on the compressible Euler equations. *Computer Methods in Applied Mechanics and Engineering*, **45**(1-3):217-284. [doi:10.1016/0045-7825(84)90157-9]

Hughes, T.J.R., Franca, L.P., Balestra, M., 1986. A new finite element formulation for computational fluid dynamics: V. Circumventing the Babuška-Brezzi condition: A stable Petrov-Galerkin formulation of the Stokes problem accommodating equal-order interpolations. *Computer Methods in Applied Mechanics and Engineering*, **59**(1):85-99. [doi:10.1016/0045-7825(86)90025-3]

Hughes, T.J.R., Franca, L.P., Hulbert G.M., 1989. A new finite element formulation for computational fluid dynamics: VIII. The Galerkin/least-squares method for advective-diffusive equations. *Computer Methods in Applied Mechanics and Engineering*, **73**(2):173-189. [doi:10.1016/0045-7825(89)90111-4]

Jiang, C.B., Kawahara, M., 1993. A three step finite element method for unsteady incompressible flows. *Computational Mechanics*, **11**(5-6):355-370. [doi:10.1007/BF00350093]

Jyotsna, R., Vanka, S.P., 1995. Multigrid calculation of steady, viscous flow in a triangular cavity. *Journal of Computational Physics*, **122**(1):107-117. [doi:10.1006/jcph.1995.1200]

Kjellgren, P., 1997. A semi-implicit fractional step finite element method for viscous incompressible flows. *Computational Mechanics*, **20**(6):541-550. [doi:10.1007/s004660050274]

Kohno, H., Bathe, K.J., 2006. A flow-condition-based interpolation finite element procedure for triangular grids. *International Journal for Numerical Methods in Fluids*, **51**(6):673-699. [doi:10.1002/fld.1246]

Oñate, E., 1998. Derivation of stabilized equations for advective-diffusive transport and fluid flow problems. *Computer Methods in Applied Mechanics and Engineering*, **151**(1-2):233-267. [doi:10.1016/S0045-7825(97)00119-9]

Oñate, E., Valls, A., Garcia, J., 2007. Modeling incompressible flows at low and high Reynolds numbers via a finite calculus-finite element approach. *Journal of Computational Physics*, **224**(1):332-351. [doi:10.1016/j.jcp.2007.02.026]

Ribbens, C.J., Watson, L.T., 1994. Steady viscous flow in a triangular cavity. *Journal of Computational Physics*, **112**(1):173-181. [doi:10.1006/jcph.1994.1090]

Selmin, V., Donea, J., Quartapelle, L., 1985. Finite element methods for nonlinear advection. *Computer Methods in Applied Mechanics and Engineering*, **52**(1-3):817-845. [doi:10.1016/0045-7825(85)90016-7]

Tezduyar, T.E., 2007a. Finite elements in fluids: Stabilized formulations and moving boundaries and interfaces. *Computers & Fluids*, **36**(2):191-206. [doi:10.1016/j.compfluid.2005.02.011]

Tezduyar, T.E., 2007b. Finite elements in fluids: Special methods and enhanced solution techniques. *Computers & Fluids*, **36**(2):207-223. [doi:10.1016/j.compfluid.2005.02.010]

Tezduyar, T.E., Ganjoo, D.K., 1986. Petrov-Galerkin formulations with weighting functions dependent upon spatial and temporal discretization: Applications to transient convection-diffusion problems. *Computer Methods in Applied Mechanics and Engineering*, **59**(1):49-71. [doi:10.1016/0045-7825(86)90023-X]

Zienkiewicz, O.C., Codina, R., 1995. A general algorithm for compressible and incompressible flow. Part I: The split characteristic based scheme. *International Journal for Numerical Methods in Fluids*, **20**(8-9):869-885. [doi:10.1002/fld.1650200812]

Zienkiewicz, O.C., Morgan, K., Satya Sai, B.V.K., Codina, R., Vazquez, M., 1995. A general algorithm for compressible and incompressible flow. Part II: Tests on the explicit form. *International Journal for Numerical Methods in Fluids*, **20**(8-9):887-913. [doi:10.1002/fld.1650200813]